

Stochastic Models of SLC HR SAR Images

Matteo Soccorsi and Mihai Datcu
German Aerospace Center
Remote Sensing Technology Institute
Oberpfaffenhofen, D-82234 Germany
Email: matteo.soccorsi@dlr.de

Abstract—The paper presents two algorithms for texture primitive feature extraction on Single Look Complex (SLC) and Polarimetric Synthetic Aperture Radar (PolSAR) SLC data. We assume the data to be modeled by a Gauss-Markov Random Field (GMRF): a complex GMRF model for characterizing the spatial correlation in SLC data and an extension of the model for inter-band correlation characterization. The complex GMRF characterizes the spatial relationship of a two-dimensional complex signal, i.e. SLC SAR data. The extended model characterizes the spatial interaction and the inter-band pixels correlation between the polarimetric complex channels. The Bayesian approach permits to deal with model fitting and selection in a direct way. The results are presented on a polarimetric E-SAR L band scene of Mannheim, Germany.

I. INTRODUCTION

High Resolution (HR) Synthetic Aperture Radar (SAR) images are two-dimensional complex signals and reveal structures both in amplitude and phase. In the case of PolSAR data each pixel is described by four complex-values. There are many contributions available in the literature dealing with PolSAR data. In [1], the principle of speckle filtering in polarimetric data is reconsidered, rising from the fact that all the scalar and most of the vectorial filters do not preserve the polarimetric information. Thus, the necessity appears to redefine the concept of speckle filtering in polarimetry, showing that all the usual polarimetric entities can be noise reduced if and only if all the elements of the Mueller matrix are filtered. Hence, they developed an extended version of the Minimum Mean Squared Error (MMSE) to estimate the unspeckled covariance matrix elements, exploiting the linear relationship between the Mueller matrix and the scattering covariance matrix. In [2], the Probability Density Functions (PDFs) for the co-polar and cross-polar ratios and for the co-polar phase in the multilook case are outlined first under the assumption of Gaussian scattering-matrix statistics, and then for a K-distribution model. The enhancement in the estimation of the polarimetric signature coefficients is demonstrated in case of *multilook signature* estimates compared with *signature averaging* estimates. Similarly, in [3], PDFs of the multilook phase differences, magnitudes of complex products, and intensity and amplitude ratios are derived. On the other hand, the statistical characteristics of multilook data are quite different from those of single-look data. In [4], the sensitivity of the normalized second

moment of the intensity on the polarization state is investigated and the polarimetric texture signature definition is introduced. In [5], an extended Polarimetric Whitening Filter (PWM) on multilook data (MPWM) is developed under the simplified hypotheses of *product model* and fully developed speckle. In addition, different estimators are compared in case of the *a priori* distribution of the texture being known or unknown. In [6], the polarization scattering properties of each pixel are classified in a unsupervised way depending on even or odd number of reflections or diffuse scattering. A more discriminative method of unsupervised analysis for polarimetric SAR data is presented in [7], where the polarimetric backscatter classes are selected based on a multi-dimensional fuzzy clustering of the logarithm of the parameters composing the polarimetric covariance matrix. In [8] an unsupervised classification method is developed starting from the supervised algorithm in [11] and giving as input of each iteration the training set obtained from the previous classification and as initialization the unsupervised classification based on polarimetric target decomposition proposed in [12]. The iterations stop when the number of pixels switching classes become smaller than a threshold number or when another convergence criteria is met. A combined method, preserving the scattering properties, is presented by [10]. It is based on the iterative Wishart classifier, after a previous decomposition of the pixels into three scattering categories [13]. Up to date, the exploitation of the contextual information directly on complex polarimetric data is not available in the literature. In [9], a segmentation followed by a classification, both based on the contextual information provided by the GMRF model, are performed on SAR polarimetric detected images for the discrimination of vegetated areas. The task is to characterize the texture, i.e. the spatial properties of the signal, by texture parameter estimation from the polarimetric complex signals. The contribution of this study is the application of the complex GMRF for feature extraction to complex PolSAR data and its comparison with a multi-dimensional GMRF for spatial and inter-band feature extraction. The comparison has been done by k-means unsupervised classification. In the following, a short overview of the two models/algorithms will be presented with their application and the obtained results.

II. BAYESIAN INFERENCE

The Bayesian modeling allows us, based on two-level inference, to perform model fitting and model selection.

The first level of inference assumes that the models to be inverted are true. The task consists in fitting the model to the data.

The Bayes' rule:

$$p(\boldsymbol{\theta}|\mathbf{x}_s, H_i) = \frac{p(\mathbf{x}_s|\boldsymbol{\theta}, H_i)p(\boldsymbol{\theta}|H_i)}{p(\mathbf{x}_s|H_i)} \quad (1)$$

is applied to the parameters $\boldsymbol{\theta}$ of the chosen model H_i , in order to obtain the probability distribution function (pdf) of the model parameter vector $\boldsymbol{\theta}$ given the data \mathbf{x}_s and the chosen model H_i . In (1) $p(\boldsymbol{\theta}|H_i)$ is the prior and $p(\mathbf{x}_s|\boldsymbol{\theta}, H_i)$ is the likelihood, of the data.

The inference process is performed through the MAP estimate:

$$\hat{\boldsymbol{\theta}}_{\text{MAP}} = \arg \max_{\boldsymbol{\theta}} \{\log p(\mathbf{x}_s|\boldsymbol{\theta}) + \log p(\boldsymbol{\theta})\} \quad (2)$$

which gives the estimated values of the model parameters.

In the notation of (2) we dropped the dependence on the model H_i . At this level of inference, the evidence term $p(\mathbf{x}_s|H_i)$ can be neglected because it is a constant term.

The task of the second level of Bayesian inference is to find the most plausible model explaining the data. At his level of inference the evidence term becomes essential. Since, in general, the model H_i is available as a forward model $p(\mathbf{x}_s|\boldsymbol{\theta}, H_i)$ of the data, the evidence is obtained by marginalization:

$$p(\mathbf{x}_s|H_i) = \int_{\Theta} p(\mathbf{x}_s|\boldsymbol{\theta}, H_i)p(\boldsymbol{\theta}|H_i)d\boldsymbol{\theta} \quad (3)$$

where the integral is in the parameter space Θ for which we denote the volume element with $d\boldsymbol{\theta}$ and the prior of the parameters with $p(\boldsymbol{\theta}|H_i)$. The evidence is a quantitative measure of how good the model fits the data and it is useful for model selection.

III. COMPLEX GMRF MODEL

Given a complex random variable $x = x_{re} + jx_{im}$, e.g. a complex-valued image pixel, the conditional GMRF pdf has the form:

$$p(x_s|\mathcal{N}_s, \boldsymbol{\theta}) = \frac{1}{\pi\sigma^2} \exp\left\{-\frac{|x_s - \eta|^2}{\sigma^2}\right\} \quad (4)$$

$$\begin{aligned} \eta = & \sum_{m,n \in \mathcal{N}_s} \theta_{mn, re}(x_{mn} + x'_{mn}) + \\ & + \frac{\theta_{mn, im}}{2}(\bar{x}_{mn} - \bar{x}'_{mn} + jx_{mn} - jx'_{mn}) \end{aligned} \quad (5)$$

where $\bar{\cdot}$ is the complex conjugate, the indexing mn and \cdot' refer to the neighborhood system of Fig. 1 and σ^2 is the variance of the process. Equation (4) is the distribution of a circular complex Gaussian process. The factor 1/2 in (5), for the imaginary part of the parameters, comes from the definition of the cross cliques under the hypothesis of reciprocity.

The Hammersley-Clifford theorem, which states the equivalence between Gibbs Random Fields and GMRF, allows to write the GMRF conditional PDFs in the form of (4) as the

	x_{44}	x_{32}	x'_{41}	
x_{43}	x_{22}	x_{12}	x'_{21}	x'_{42}
x_{31}	x_{11}	x_s	x'_{11}	x'_{31}
x_{42}	x_{21}	x'_{12}	x'_{22}	x'_{43}
	x_{41}	x'_{32}	x'_{44}	

Fig. 1. Example of neighborhood \mathcal{N}_s . x_s is the center of the neighborhood, the same subindex marks the pixels belonging to the same clique system and the prime \cdot' denotes the symmetry of the neighborhood with $x_{mn} = x'_{mn}$.

value of each pixel depends only on a limited number of surrounding pixels belonging to the neighborhood \mathcal{N}_s .

IV. MULTI-DIMENSIONAL GMRF

The multi-dimensional GMRF model comes from the classical definition of auto-regressive processes to estimate the parameters of a Markovian chain:

$$x_s = \sum_{m,n \in \mathcal{N}_s} \theta_{mn}(x_{mn} + x'_{mn}) + n_s \quad (6)$$

The extension over the third dimension is obtained by defining a certain number of cliques across the bands. Considering the central band in a set of three bands, the number of centers for a pixel belonging to the reference band is equal to three for model order one and to nine for a second order model.

Under the hypotheses of ergodic processes and stationary signals in the analyzing window, a sufficient number of samples over the third dimension can be collected. A cross-band parameter is obtained by spatial averaging of the clique in the analyzing window.

V. MAP ESTIMATOR

Using a matrix formalism we can rewrite (6) as follows:

$$\begin{aligned} \mathbf{x}_s &= \mathbf{G}\boldsymbol{\theta} + \mathbf{n}_s \\ \mathbf{x}_s, \mathbf{G}, \mathbf{n}_s &\in \mathbb{C} \\ \boldsymbol{\theta} &\in \mathbb{R} \end{aligned} \quad (7)$$

where \mathbf{G} is the matrix of the cliques, $\boldsymbol{\theta}$ is the parameter vector and \mathbf{x}_s is the noisy image. The \mathbf{G} matrix has $P \times Q$ elements where P is the number of the non-border pixels and Q is the total number of parameters to be estimated.

Based on the following assumptions:

- the symmetry of the Gaussian pdf ensures that the $\hat{\boldsymbol{\theta}}_{\text{MAP}}$ estimate equals the LSE $\hat{\boldsymbol{\theta}}_{\text{LSE}}$, and
- the covariance matrix of the noise \mathbf{n} is equal to the identity complex matrix,

where the latter assumption comes from the fact that we can make the simplest allowed assumption.

Thus, they result in the equivalence between a MAP estimate and LSE, which takes the form:

$$\hat{\theta} = (\mathbf{G}^H \mathbf{G})^{-1} \mathbf{G}^H x_s \quad (8)$$

where \cdot^H is the Hermitian operator and $\hat{\theta}$ is the estimated parameter vector.

The pseudo-inverse matrix $(\mathbf{G}^H \mathbf{G})^{-1}$ represents the complex covariance matrix of the model.

VI. RESULTS

The results are presented for an E-SAR scene of the city of Mannheim, Germany. All the full complex polarimetric data are available, acquired in L band with azimuth resolution 1.2 m and range resolution 1.99 m.

We selected a representative part of the scene, shown in Fig. 2.

Under the hypothesis of reciprocity, we neglected the cross-polarization VH band and we analyzed the HH-VV-HV full complex bands.

We processed each band separately by complex GMRF with model order two and an analyzing window size of 35×35 pixels. Then, we joined all the parameters and we classified the feature space through unsupervised k-means classification fixing the number of classes to five.

For the analysis by multi-dimensional GMRF the order of the bands is important because the central one is used as reference. We chose the order HH-VV-HV because the coherence between the co-polar bands is higher than between the co-polar/cross-polar bands. Thus, we guess to extract more information through this configuration. Nevertheless, further analyses are going to be carried out in order to ascertain the correct band arrangement.

We analyzed the data with an analyzing window of 35×35 pixels and we got nine parameters from the multi-dimensional analysis. Once more, we classified the feature space through an unsupervised k-means classifier with the same setup.

The classification results are shown in Fig. 2. We provide also the classification performed on the parameters extracted only from the HH complex band.

An unsupervised classification is automatically performed by the classifier which is building the class without any reference or training data, thus we verified the result by Google Earth ground truth.

The five classes, within the limit of the sensor resolution and the analyzing window size, correspond to water (white), non-built area (pink and blue), residential area (green) and strong scatterers (black). The classifications appear similar but details are better discriminated for the multi-band analysis than for the single band complex feature extraction, e.g. the strong scatterers (black) class.

VII. CONCLUSION

The paper presents two algorithms for texture feature extraction, both based on complex GMRF model.

The first model extracts feature from two-dimensional complex signals whereas the second is able to characterize the spatial

and the cross-band correlation.

The extracted parameters are compared by unsupervised classification.

The results are provided for E-SAR PolSAR image selected from a scene acquired over the city of Mannheim, Germany. The data do not present large polarization diversities due to the acquisition in L-band in the urban area.

The model selection reveals higher values for the evidence of complex GMRF model. On the other hand, it is not a full approach because it is based on the separate analysis of each band, thus the inter-band information is ignored.

In contrast, multi-dimensional GMRF collects the cross-band information even if in our case we estimate the parameters only by one configuration while a full approach would consider all potential configurations in order to capture as much information as possible.

Further steps will be to perform classifications with texture primitive feature extracted from the complex covariance matrix or Mueller matrix elements and/or to find data transformations better fitting the model.

Eventually, the classification method to assess the quality of the parameters has to be verified with alternative techniques, e.g. simulations, distance measures or image information mining system.

ACKNOWLEDGMENT

This work was carried out in the frame of the *CNES/DLR/ENST Competence Center on Information Extraction and Image Understanding for Earth Observation*. The authors would like to thank Gottfried Schwarz for his helpful hints.

REFERENCES

- [1] R. Touzi and A. Lopes, *The Principle of Speckle Filtering in Polarimetric SAR Imagery*, IEEE Trans Geosci. Remote Sens., vol. 32, n. 5, pp. 1110-1114, September 1994.
- [2] I. R. Joughin, D. P. Winebrenner and D. B. Percival, *Probability Density Functions for Multilook Polarimetric Signatures*, IEEE Trans Geosci. Remote Sens., vol. 32, n. 3, pp. 562-574, May 1994.
- [3] J.-S. Lee, K. W. Hoppel, S. A. Mango and A. R. Miller, *Intensity and Phase Statistics of Multilook Polarimetric and Interferometric SAR Imagery*, IEEE Trans Geosci. Remote Sens., vol. 32, n. 5, pp. 1017-1028, September 1994.
- [4] G. De Grandi, J.-S. Lee, D. Schuler and E. Nezry, *Texture and Speckle Statistics in Polarimetric SAR Synthesized Images*, IEEE Trans Geosci. Remote Sens., vol. 41, n. 9, pp. 2070-2088, September 2003.
- [5] A. Lopès and F. Séry, *Optimal Speckle Reduction for the Product Model in Multilook Polarimetric SAR Imagery and the Wishart Distribution*, IEEE Trans Geosci. Remote Sens., vol. 35, n. 3, pp. 632-647, May 1997.
- [6] J. J. Van Zyl, *Unsupervised Classification of Scattering Behavior Using Radar Polarimetry Data*, IEEE Trans Geosci. Remote Sens., vol. 27, n. 1, pp. 36-45, January 1989.
- [7] E. Rignot, R. Chelappa and P. Dubois, *Unsupervised Segmentation of Polarimetric SAR Data Using the Covariance Matrix*, IEEE Trans Geosci. Remote Sens., vol. 30, n. 4, pp. 697-705, July 1992.
- [8] J.-S. Lee, M. R. Grunes, T. L. Ainsworth, L.-J. Du, D. L. Schuler and S. R. Cloude, *Unsupervised Classification Using Polarimetric Decomposition and the Complex Wishart Classifier*, IEEE Trans Geosci. Remote Sens., vol. 37, n. 5, pp. 2249-2258, September 1999.
- [9] Y. Dong, A. K. Milne and B. C. Forster, *Segmentation and Classification of Vegetated Areas Using Polarimetric SAR Image Data*, IEEE Trans Geosci. Remote Sens., vol. 39, n. 2, pp. 321-329, February 2001.

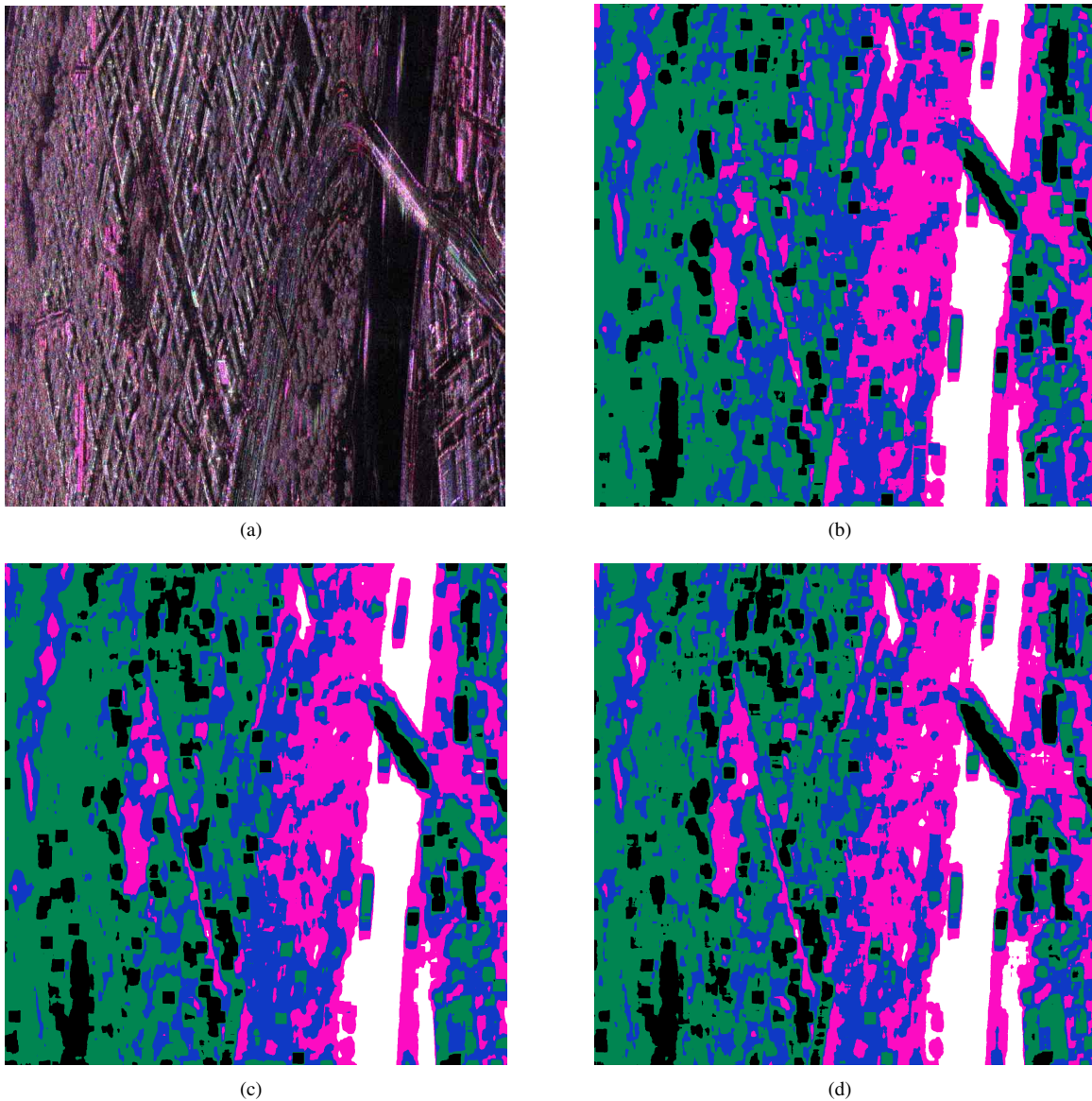


Fig. 2. RGB (R=HH, G=HV, B=VV) color PolSAR image, L band, acquired over the city of Mannheim, Germany (a) and classification results (b), (c), (d). Complex GMRF based classification for the parameters extracted from band HH (b). Complex GMRF based classification for the parameters extracted from band HH, VV and HV (c). Multi-dimensional GMRF based classification for the configuration HH-VV-HV (d). The classifications appear to be similar, but slightly more details are preserved in the classification based on the multi-dimensional model. It is notable for the strong scatterers class (black).

- [10] J.-S. Lee, M. R. Grunes, E. Pottier and L. Ferro-Famil, *Unsupervised Terrain Classification Preserving Polarimetric Scattering Characteristics*, IEEE Trans Geosci. Remote Sens., vol. 42, n. 4, pp. 722-731, April 2004.
- [11] J.-S. Lee, M. R. Grunes and R. Kwok, *Classification of Multi-Look Polarimetric SAR imagery based on Complex Wishart Distribution*, Int. J. Remote Sensing, vol. 15, n. 11, pp. 2299-2311, November 1994.
- [12] S. R. Cloude and E. Pottier, *An Entropy based classification scheme for land application of polarimetric SAR*, IEEE Trans Geosci. Remote Sens., vol. 35, n. 1, pp. 68-78, January 1997.
- [13] A. Freeman and S. L. Durden, *A Three-Component Scattering Model for Polarimetric SAR Data*, IEEE Trans Geosci. Remote Sens., vol. 36, no. 3, pp. 963-973, May 1998.